nature sustainability

Article

https://doi.org/10.1038/s41893-024-01363-1

Efficient CO and acrolein co-production via paired electrolysis

Received: 26 June 2023

Accepted: 26 April 2024

Published online: 29 May 2024

Check for updates

Xue Wang[1,2,6], Peihao Li[1,6], Jason Tam[3], Jane Y. Howe[3,4], Colin P. O'Brien[5], Armin Sedighian Rasouli[1], Rui Kai Miao[5], Yuan Liu[1], Adnan Ozden[5], Ke Xie[1], Jinhong Wu[5], David Sinton[5] & Edward H. Sargent[1]

Paired electrolysis—the combination of a productive cathodic reaction, such as CO_2 electroreduction (CO_2RR), with selective oxidation on the anode—provides an electrified reaction with maximized atom and energy efficiencies. Unfortunately, direct electro-oxidation reactions typically exhibit limited Faradaic efficiencies (FEs) towards a single product. Here we apply paired electrolysis for acidic CO_2RR and the model organic oxidation allyl alcohol oxidation reaction to acrolein. This CO_2RR alcohol oxidation reaction system shows (96 ± 1)% FE of CO_2 to CO on the cathode and (85 ± 1)% FE of allyl alcohol to acrolein on the anode. As a result of this pairing with organic oxidation on the anode, the full-cell voltage of the system is lowered by 0.7 V compared with the state-of-art acidic CO_2-to-CO studies at the same 100 mA cm^{-2} current density. The acidic cathode avoids carbonate formation and enables a single-pass utilization of CO_2 of 84% with a 6× improvement in the atom efficiency of CO_2 utilization. Energy consumption analysis suggests that, when producing the same amount of CO, the system reduces energy consumption by an estimated 1.6× compared with the most energy-efficient prior acidic CO_2-to-CO ambient-temperature electrolysis systems. The work suggests that paired electrolysis could be a decarbonization technology to contribute to a sustainable future.

The carbon dioxide electroreduction reaction (CO_2RR) powered using low-carbon electricity provides one route to chemicals and fuels[1]. Recently, this field has seen impressive advances in respect of selectivity and current density[2–12]. Nevertheless, CO_2RR still suffers from challenges that include (bi)carbonate formation when alkaline/neutral electrolytes are employed, low CO_2 utilization (that is, low atom efficiency) and high full-cell voltage[13–15]. To produce CO in CO_2RR via a two-electron-transfer process, the upper bound on CO_2 utilization is 50% in neutral electrolyte, and it is lower still in alkaline conditions because CO_2 is lost to the electrolyte[16,17].

CO_2RR in acidic media addresses the CO_2 loss issue resulting from (bi)carbonate formation and crossover in alkaline or neutral media during reaction. As a result, it increases the CO_2 utilization. Challenging, though, is the kinetically favoured hydrogen evolution reaction (HER) in acidic media[18–21]. In recent years, several studies have reported CO_2RR in acidic media with the suppression of HER at relevant current densities above 100 mA cm^{-2} (ref. 22–26); however, the full-cell voltage required in previously reported acidic CO_2RR systems has been high, typically ~4 V (refs. 23,24), corresponding to high energy consumption.

Most CO_2RR studies pair with the oxygen evolution reaction (OER) on the anode (CO_2RR-OER systems)[2–12,18–26]. The standard potential of OER is 1.23 V versus reversible hydrogen electrode (RHE)[27], and O_2 offers limited economic value. This motivates interest in CO_2RR paired with an efficient anodic reaction that requires a lower thermodynamic

[1]Department of Electrical and Computer Engineering, University of Toronto, Toronto, Ontario, Canada. [2]School of Energy and Environment, City University of Hong Kong, Kowloon, Hong Kong, China. [3]Department of Materials Science and Engineering, University of Toronto, Toronto, Ontario, Canada. [4]Department of Chemical Engineering and Applied Chemistry, University of Toronto, Toronto, Ontario, Canada. [5]Department of Mechanical and Industrial Engineering, University of Toronto, Toronto, Ontario, Canada. [6]These authors contributed equally: Xue Wang, Peihao Li. e-mail: ted.sargent@utoronto.ca

https://doi.org/10.1038/s41893-024-01363-1

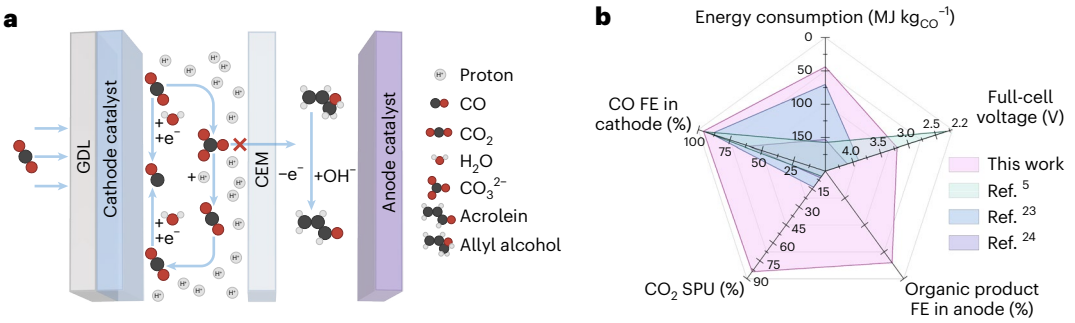

Fig. 1 | A paired electrolysis system co-producing CO and acrolein. a, A schematic of the paired electrolysis system consisting of CO_2-to-CO at the cathode and allyl alcohol-to-acrolein at the anode. **b**, A comparison of product selectivities at the cathode and anode, full-cell potential, CO_2 SPU and energy consumption in this work with those of state-of-the-art CO_2-to-CO ambient-temperature electrolysis systems.

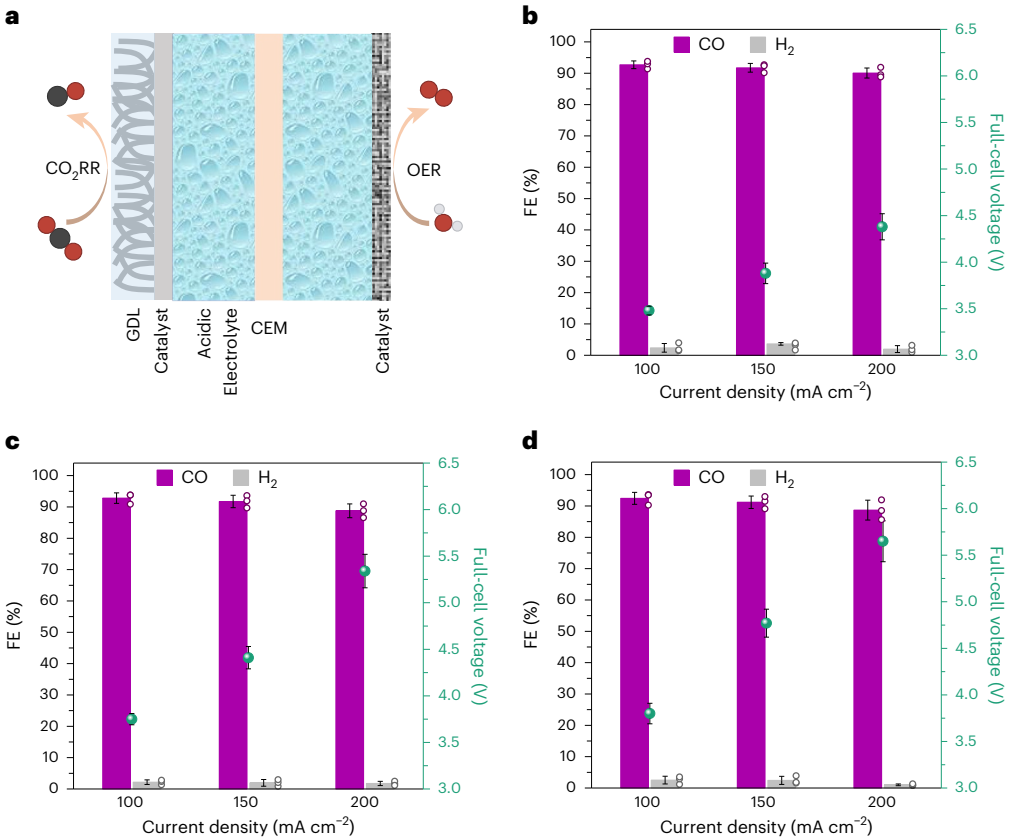

Fig. 2 | CO_2RR performance in the CO_2RR-OER system. a, A schematic of the CO_2RR-OER system. **b**–**d**, The CO_2RR gas product distribution on 500 nm sputtered Ag/GDL in 3 M KCl electrolytes, and full-cell voltage of the CO_2RR-OER system under different current densities adjusted by H_2SO_4 to pH 1 (**b**), 2 (**c**) and 3 (**d**) in the CO_2RR-OER system. In **b**–**d**, the error bars of the FEs represent the standard deviation of three independent samples and the data are presented as mean values ± standard deviation with an n of 3. The error bars of the full-cell voltages represent the standard deviation of potentials (n = 600) during the constant current electrolysis for 10 min, and the data are presented as mean values ± standard deviation.

potential, such as selective oxidation of organics[27–29]. Until now, however, such anodic reactions have typically seen modest Faradaic efficiency (FE) when operated near ambient conditions[30,31].

In this Article, we report a paired electrolysis system with low energy consumption (Fig. 1a): cathodic CO_2RR to CO in acidic media coupled to anodic allyl alcohol oxidation reaction (AOR) to acrolein. In this paired electrolysis system, we achieve a CO FE of (96 ± 1)% at the cathode and acrolein FE of (85 ± 1)% at the anode at 100 mA cm^{-2} (Fig. 1b). When it is optimized for single-pass utilization (SPU), the cathode reaches a CO_2 SPU of 84%, fully a 6× improvement compared with the highest SPU value reported in prior acidic CO_2-to-CO studies undertaken above 100 mA cm^{-2} (Supplementary Table 1). The full-cell voltage averages to 3.2 V over the course of 10 h operation, and the energy consumption for producing 1 kg of CO in this paired electrolysis system is 44 MJ, representing a decrease in the voltage of 0.7 V and a reduction of 1.6× in energy consumption relative to the most energy-efficient prior reported acidic ambient-temperature CO_2-to-CO studies.

Results

CO_2 electroreduction in acidic media

We began by exploring CO_2RR in acidic media coupled to OER. Ag is known (from prior neutral and alkaline studies) for its selectivity to

https://doi.org/10.1038/s41893-024-01363-1

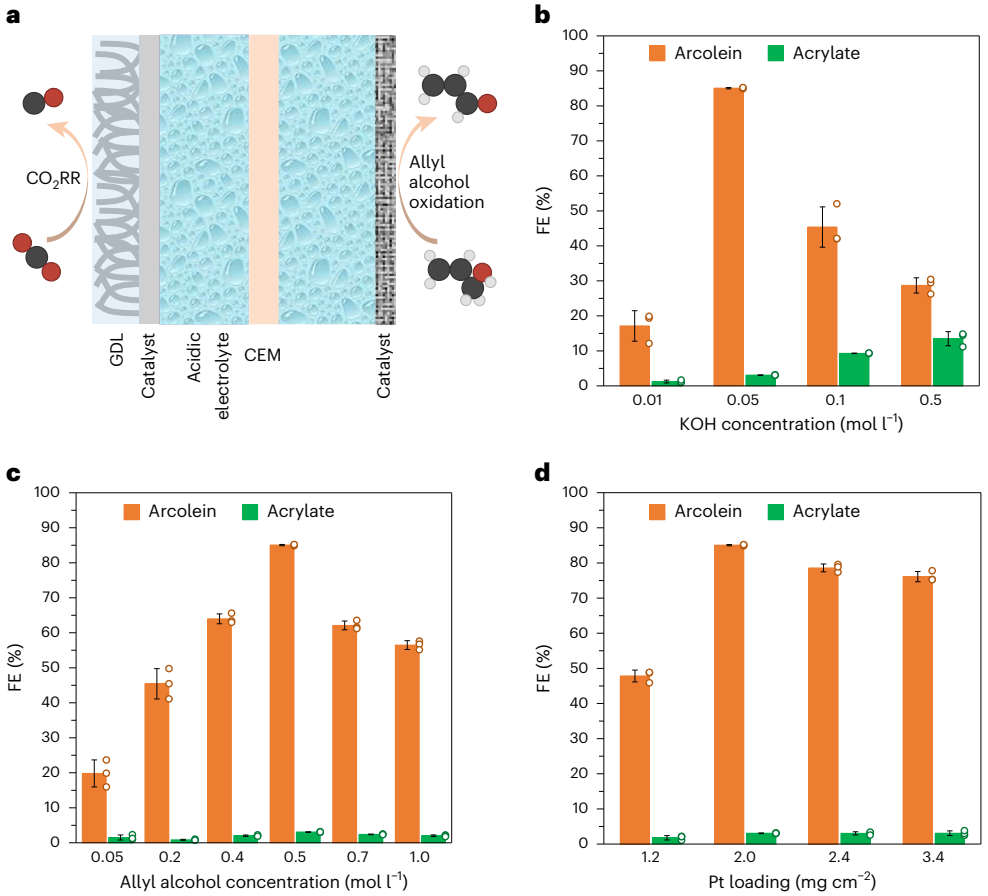

Fig. 3 | AOR performance in the CO_2RR-AOR system. a, A schematic of the CO_2RR-AOR system. **b**, The AOR performance in 0.5 M allyl alcohol electrolyte containing different concentrations of KOH at 100 mA cm^{-2}. **c**, The AOR performance in 0.05 M KOH electrolyte containing different concentrations of allyl alcohol at 100 mA cm^{-2}. **d**, The AOR performance in 0.5 M allyl alcohol + 0.05 M KOH electrolyte at 100 mA cm^{-2} using anode electrodes with different Pt loadings. The catholyte in **b**–**d** is 3 M KCl adjusted to pH 1 using H_2SO_4. In **b**–**d**, the error bars represent the standard deviation of three independent samples and the data are presented as mean values ± standard deviation with an *n* of 3.

CO (ref. 17). We fabricated Ag cathodes by sputtering a layer of Ag on a carbon-based gas diffusion layer (Ag/GDL). Scanning electron microscopy (SEM) (Supplementary Fig. 1a,b) shows that the Ag layer consists of nanoparticles. Powder X-ray diffraction (XRD) pattern and X-ray photoelectron spectroscopy (XPS) of the cathode show the catalyst on the GDL is crystalline metallic Ag (Supplementary Fig. 1c,d). The anode electrode was prepared by spray coating commercial carbon-supported Pt nanoparticles with a size of ~5 nm (Supplementary Fig. 2) on Ti fibre felt (Methods).

We used a flow cell electrolyser in a two-electrode configuration (Supplementary Fig. 3) for electrolysis. As illustrated in Fig. 2a, on the cathode, we used an acidic electrolyte prepared using 3 M KCl electrolyte adjusted using H_2SO_4. The use of acidic electrolyte on the cathode enables a cation exchange membrane (CEM), avoiding carbonate crossover and, hence, preventing CO_2 evolution on the anode, but reliance on acidic electrolyte requires a strategy to suppress HER and activate CO_2RR, something we achieve using K^+ ions (we used 3 M KCl) added to the acidic catholyte[22,25,32]. For bulk pH 1–3, the CO FEs are ~90% and the H_2 FEs are below 3% on 500 nm sputtered Ag/GDL in the current density range 100–200 mA cm^{-2} (Fig. 2b–d, Supplementary Fig. 4 and Supplementary Table 2). Three-hundred nanometres sputtered Ag/GDL also delivered CO FE of ~90% in the range 100–200 mA cm^{-2} under bulk pH of 1 (Supplementary Fig. 5). In this CO_2RR-OER system, we achieve a full-cell voltage of 3.5 V—without correction—at 100 mA cm^{-2} in electrolyte having pH 1 (Fig. 2b).

Paired electrolysis of CO_2RR and AOR

We then sought to switch the anodic reaction to organic oxidation paired with the above cathode (Fig. 3a). We selected allyl alcohol oxidation since, in the ideal case, a CO_2RR-AOR system has a lower potential compared with idealized CO_2RR-OER. Allyl alcohol is available via the formic acid-mediated deoxydehydration of glycerol[33], and acrolein is a feedstock for acrylic acid[34].

We first investigated the feasibility of performing anodic AOR in acidic media. Acidic anolytes of different bulk pHs consist of 0.5 M allyl alcohol and different concentrations of H_2SO_4 and K_2SO_4 (0.2 M H_2SO_4 for pH 0.8, 0.05 M H_2SO_4 for pH 1.3, and 0.1 M K_2SO_4 for pH 5.4). Attractively, by switching OER to AOR in the anode, the full-cell voltages were reduced to the 2.7–2.8 V range at 100 mA cm^{-2} (Supplementary Fig. 6a). However, the liquid products—acrolein and acrylic acid—following AOR were produced with FEs below 2% at 100 mA cm^{-2} quantified by high-performance liquid chromatography (HPLC) (Supplementary Fig. 6b).

We then studied anodic AOR in alkaline media. Here, we found that acrolein generation is promoted compared with that in acidic media and that the choice of anolyte affects selectivity in allyl alcohol oxidation. Seeking optimized alkaline anolyte conditions for AOR, we screened a series of anolytes with different concentrations of allyl alcohol and KOH in the CO_2RR-AOR system, wherein we evaluated simultaneously the cathodic CO_2RR performance and anodic AOR performance (Fig. 3b,c and Supplementary Tables 3 and 4). On the

https://doi.org/10.1038/s41893-024-01363-1

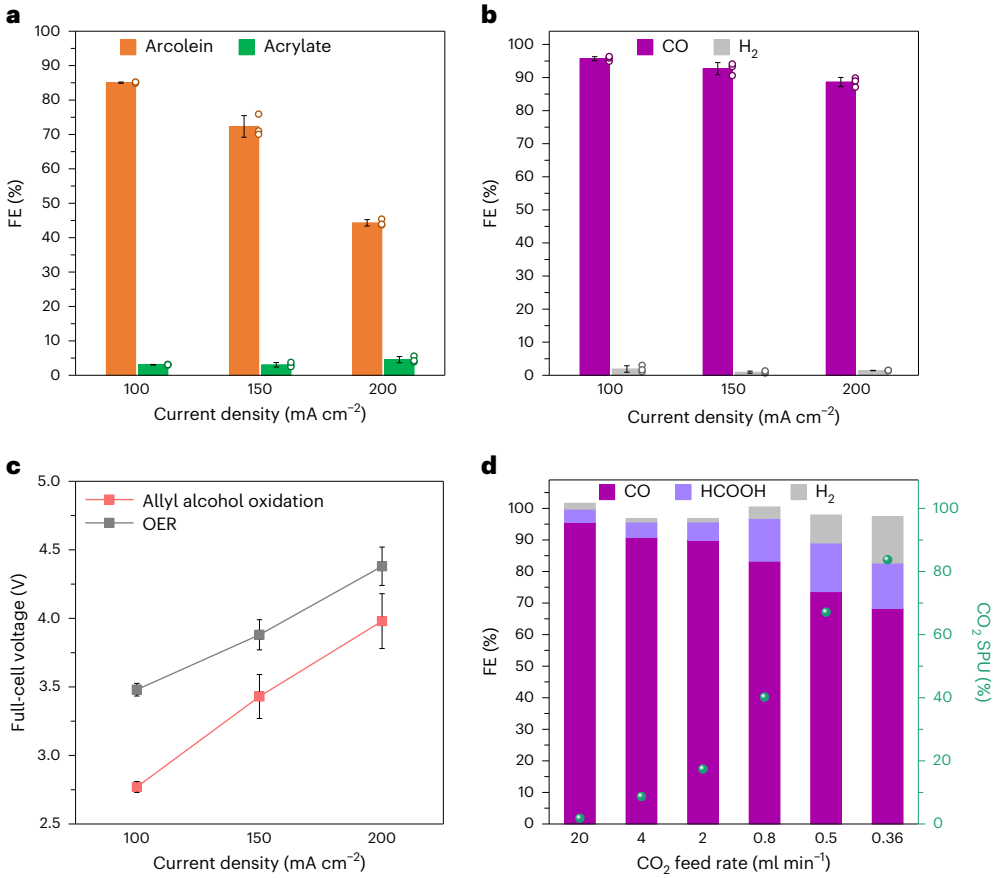

Fig. 4 | AOR and CO_2RR performance in the CO_2RR-AOR system. a, The AOR performance in 0.5 M allyl alcohol + 0.05 M KOH electrolyte under different current densities. **b**, The CO_2RR gas product distribution under different current densities in the CO_2RR-AOR system. Anolyte: 0.5 M allyl alcohol + 0.05 M KOH. In **a** and **b**, the error bars represent the standard deviation of three independent samples and the data are presented as mean values ± standard deviation with a number of 3. **c**, A full-cell voltage comparison between the CO_2RR-AOR system (anolyte: 0.5 M allyl alcohol + 0.05 M KOH) and the CO_2RR-OER system (anolyte: 0.05 M KOH) under different current densities. The error bars represent the standard deviation of potentials (n = 600) during the constant current electrolysis for 10 min. The data are presented as mean values ± standard deviation. **d**, The FEs of CO, formic acid and H_2, as well as CO_2 SPU with different CO_2 feed rates at 100 mA cm^{-2}. The catholyte in **a**–**d** is 3 M KCl adjusted to pH 1 using H_2SO_4.

cathode, at 100 mA cm^{-2}, the CO_2RR product distribution is similar among CO_2RR-AOR systems with different alkaline anolytes, and the main product is CO, with FE >90% (Supplementary Tables 3 and 4). However, the selectivity towards acrolein and acrylate on the anode depends on the alkaline anolyte. We optimized the concentration of KOH and allyl alcohol in the anolyte and obtained an acrolein FE of (85 ± 1)% and an acrylate FE of (3 ± 1)% at 100 mA cm^{-2} under 0.5 M allyl alcohol + 0.05 M KOH anolyte (Fig. 3b,c). In HPLC, in addition to peaks assigned to acrolein, acrylate and allyl alcohol, there exist peaks between acrolein and acrylate (Supplementary Fig. 7). Nuclear magnetic resonance (NMR) and gas chromatography–mass spectrometry analyses demonstrated that there are small amounts of allyl glycidyl ether, 3-hydroxypropionaldehyde, 1,3,3-propanetriol, 3-hydroxypropionate, propionate, 2-(oxiran-2-ylmethoxymethyl) oxirane and 2,3-dimethylidenebutane-1,4-diol (Supplementary Figs. 8 and 9); these taken together account for ~12% total FE.

To explore the effect of the catalyst on the anodic AOR performance, we screened a series of carbon-supported metal catalysts with different metal loadings—from 1.2 to 3.4 mg cm^{-2}—in allyl alcohol oxidation, including Pt, Pd, Ru and Au (Fig. 3d and Supplementary Figs. 10–16). The anodes were prepared via the same spray coating approach. Among these anodes, the Pt anode with 2.0 mg cm^{-2} Pt loading delivers the highest acrolein FE of (85 ± 1)% at 100 mA cm^{-2} with allyl alcohol conversion of 15% following 10 min of electrolysis using 0.5 M allyl alcohol + 0.05 M KOH anolyte (Fig. 3d, Supplementary Table 5 and Supplementary Figs. 17–19).

Under the optimized condition at the anode determined via the studies above—0.5 M allyl alcohol + 0.05 M KOH anolyte and anode electrode with 2.0 mg cm^{-2}—we further evaluated the performance of CO_2RR-AOR system in the regime of 100–200 mA cm^{-2} (Fig. 4, Supplementary Fig. 20 and Supplementary Table 6). With the increase in the current density, the selectivity towards the main product, acrolein at the anode and CO at the cathode, declined (Fig. 4a,b). At 100 mA cm^{-2}, we achieved a CO FE of (96 ± 1)% in CO_2RR—comparable to other high-performance acidic CO_2-to-CO reports[23,25,35]—and the highest acrolein FE of (85 ± 1)% in AOR. At the same current density, the full-cell voltage of CO_2RR-AOR system decreased compared with that of the CO_2RR-OER system (Fig. 4c).

To reduce the energy consumption of gas product separation after CO_2RR, we pursued a high CO_2 SPU in the CO_2RR-AOR system. We varied the CO_2 feed rate, achieving CO_2 SPU of 84% at 100 mA cm^{-2}. This is 6× higher than in the highest-SPU prior reports of acidic CO_2-to-CO that were done above 100 mA cm^{-2} (Supplementary Table 1)[22–25,35], while maintaining a total C_1 FE of 83% in CO_2RR under the CO_2 feed rate of 0.36 ml min^{-1} (Fig. 4d) and achieving an acrolein FE of 85% in AOR. In addition, we note that CO FE declined with the decrease in CO_2 feed rates while the CO_2 SPU increased. System optimization can be carried out to select the best combination of CO FE and CO_2 SPU. We also

https://doi.org/10.1038/s41893-024-01363-1

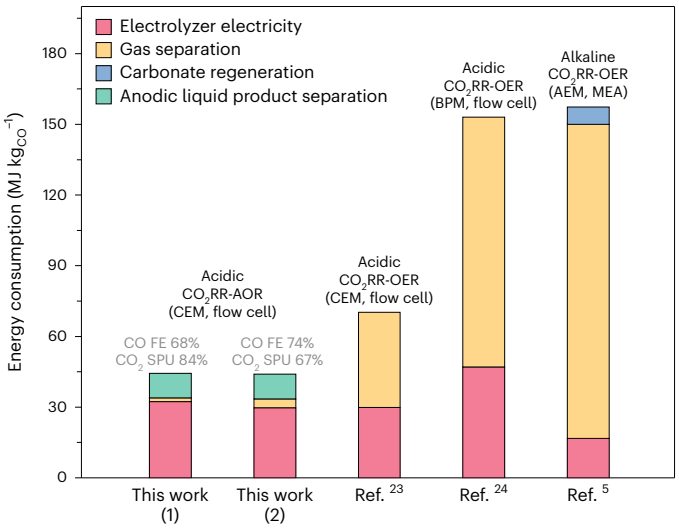

Fig. 5 | Comparison of estimated energy consumption for the production of 1 kg of CO. For CO_2RR-AOR systems, the energy consumption for AOR liquid product separation is included. BPM, bipolar membrane; AEM, anion exchange membrane; MEA, membrane electrode assembly.

investigated the CO_2 SPU at 200 mA cm^{-2} (Supplementary Fig. 21). Similar to the trend seen at 100 mA cm^{-2}, CO FE diminished with the decrease of CO_2 feed rates at 200 mA cm^{-2}, and we achieved the highest CO_2 SPU of 73% at CO_2 feed rate of 0.72 ml min^{-1}.

We evaluated the overall energy consumption of producing 1 kg of CO. We sought, in the context of a paired CO_2RR-AOR system, to account for CO electroproduction, gas separation and carbonate regeneration for the recovery of CO_2 and of the alkaline electrolyte, and for liquid product separation at the anode (Fig. 5, Supplementary Tables 7 and 8, and Supplementary Text). Because the CO_2 utilization is high, the energy of separation of CO/CO_2 is reduced relative to prior reports; the use of acidic conditions avoids (bi)carbonate that leads in some prior reports to the need for separation of CO_2 on the anode gas side as well. The system studied herein requires 44 $MJ\ kg_{CO}^{-1}$, lowering energy consumption by 1.6× compared with the most energy-efficient prior systems among acidic CO_2RR-OER systems with a CEM in a flow cell[23], acidic CO_2RR-OER systems with bipolar membrane (BPM) in a flow cell[24], and alkaline CO_2RR-OER systems with an anion exchange membrane (AEM) in a membrane electrode assembly (MEA) cell[5].

We operated the optimized CO_2RR-AOR system at a current density of 100 mA cm^{-2} for 10 h (Supplementary Fig. 22). Over the course of 10 h of continuous operation, the CO_2RR-AOR system exhibits stable CO selectivity (~90%) in cathodic CO_2RR and acrolein selectivity (>82%) in anodic AOR. The full-cell voltage of the CO_2RR-AOR electrolysis system averaged to 3.2 V during 10 h of operation, 0.8 V lower relative to the corresponding CO_2RR-OER system having an averaged full-cell voltage of 4.0 V during ~ 4 h operation (Supplementary Figs. 22 and 23).

Discussion

In this work, we develop an efficient paired electrocatalysis system with low energy consumption comprising acidic CO_2-to-CO at the cathode and allyl alcohol oxidation at the anode. We achieve CO FE of (96 ± 1)% in cathodic CO_2RR and acrolein FE of (85 ± 1)% in anodic AOR at 100 mA cm^{-2}, associated with an averaged full-cell voltage of 3.2 V during 10 h operation—lowering by 0.7 V in full-cell voltage relative to the best previously reported full-cell acidic CO_2-to-CO studies. Suppressing HER in acidic environment, we achieve a high CO_2 SPU of 84% for C_1 products in CO_2RR. During 10 h operation at 100 mA cm^{-2}, our CO_2RR-AOR system delivers stable and high selectivities towards CO (~90%) in cathode and acrolein (>82%) in anode. Energy consumption analysis suggests that, compared with the most energy-efficient prior systems, this CO_2RR-AOR system reduces energy consumption by 1.6× when producing the same amount of CO.

This work indicates a route to produce chemicals efficiently at both the cathode and the anode through paired electrolysis. At the same time, it also surfaces additional areas for research in paired electrolysis. It will be of interest to identify reactions that employ the same electrolyte on each side, thus reducing the risk of changes in pH and/or metal cation concentration over the course of extended reaction studies. Similarly, continuing to identify the mechanistic contributors to overpotentials—both cathodic and anodic—will be a worthwhile effort to inform their practical minimization within coupled electrolysis systems. Producing liquid products at high concentrations remains a priority in all studies in which liquid:liquid product separation is to be anticipated, and continued progress in ultrahigh selectivities towards a single desired product is of continued interest.

Methods

Electrode preparation

The cathode electrode was prepared by sputtering Ag with different thickness onto a piece of carbon paper gas diffusion electrode (Sigracet 39 BB, Fuel Cell Store) at a rate of 1 Å s^{-1} by using a pure Ag target (99.99%). To fabricate the anode electrode, we first etched the Ti fibre felts (Fuel Cell Store) in a 10 wt.% oxalic acid aqueous solution at 98 °C for 40 min. The etched Ti fibre felts were washed by deionized water and then dried at room temperature. Commercial carbon-supported metal nanoparticles (60 wt.% Pt on vulcan XC-72R, Fuel Cell Store, 4–5 nm; 60 wt.% Pd on Vulcan XC-72R, Fuel Cell Store, 6–8 nm; 40 wt.% Ru on vulcan XC-72R, Fuel Cell Store, 4–6 nm; or 40 wt.% Au on Ketjenblack, Fuel Cell Store, 3–6 nm) were dispersed in the mixture of deionized water, isopropanol and Nafion perfluorinated resin solution (5 wt.%, Sigma-Aldrich) and ultrasonicated for 90 min. The well-dispersed suspension was then spray coated on Ti fibre felts to prepare anode electrodes with different metal loadings.

Materials characterization

SEM and transmission electron microscopy images were taken through a Hitachi FE-SEM SU8230 scanning electron microscope at 1 kV and a Hitachi HF-3300 scanning/transmission electron microscope at 300 kV, respectively. XRD was recorded on a Rigaku MiniFlex600 X-ray diffractometer with Cu-Kα radiation. XPS measurement was carried out using a PerkinElmer 5600 XPS spectrometer using a monochromatic aluminium X-ray source.

Electrochemical measurements

The electrochemical measurements were conducted using an electrochemical station (AUT5113) with a two-electrode system in a flow cell (Supplementary Fig. 3). Cathode electrodes, CEM (Nafion 117, Fuel Cell Store), and anode electrodes were positioned and clamped together via polytetrafluoroethylene gaskets. The geometric area of the cathode electrode in the flow cell is 0.49 cm^2. In the CO_2RR-OER system, 3 M KCl aqueous solution with different pHs adjusted by H_2SO_4 and 0.05 M KOH aqueous solution were introduced into the cathode chamber and anode chamber, respectively. In the CO_2RR-AOR system, 3 M KCl aqueous solution adjusted by H_2SO_4 to pH 1 as catholyte and different concentrations of allyl alcohol in KOH aqueous solution or different concentrations of H_2SO_4/K_2SO_4 as anolyte were introduced into the cathode chamber and anode chamber, respectively. The electrolytes were circulated using peristaltic pumps at the rate of 5 ml min^{-1}. CO_2 gas (Linde, 99.99%) was continually supplied to the gas chamber of the flow cell during CO_2RR (without specification, the CO_2 feed rate is 20 ml min^{-1}). During long-term operation, fresh electrolytes were continually provided to the cathode and anode chambers using peristaltic pumps. A gas chromatograph (Shimadzu GC-2014ATF) equipped with thermal conductivity and flame ionization detectors was used to examine the CO_2RR

gas products. NMR spectrometer (Agilent DD2 600 MHz) was used to analyse the liquid products generated in cathodic CO_2RR and anodic allyl alcohol oxidation with dimethylsulfoxide as an internal standard. Combined with NMR results, gas chromatography–mass spectrometry (Thermo ISQ7000) was further used to analyse all the liquid products generated in anodic allyl alcohol oxidation. The acrolein and acrylic acid/acrylate produced in anodic AOR were quantified using HPLC (Thermo Scientific DIONEX UltiMate 3000; Aminex HPX-87H 300 × 7.8 mm column) with an aqueous solution of 0.005 M H_2SO_4 as eluate.

CO_2 SPU calculation

As only CO and formic acid were generated in our system during CO_2RR, under 293.15 K and 101,325 Pa, the CO_2 SPU is calculated as

$$CO_2\mathrm{SPU} = \frac{\text{Total current [A]} \times (FE_{co}+FE_{HCOOH}) \times 60\,[\text{s}]}{2 \times \text{Faraday's constant}\left[\text{C mol}^{-1}\right]} \div \frac{\text{CO}_2\text{ feed rate}\left[\frac{\text{m}^3}{\text{min}}\right] \times 1\,[\text{min}]}{\frac{8.314\left[\text{Jmol}^{-1}\,\text{K}^{-1}\right]\times 293.15\,[\text{K}]}{101300\,[\text{Pa}]}}. \quad (1)$$

Reporting summary

Further information on research design is available in the Nature Portfolio Reporting Summary linked to this article.

Data availability

All data are available within the paper, Supplementary Information and source data file. Source data are provided with this paper.

References

1. Jhong, H.-R., Ma, S. & Kenis, P. J. A. Electrochemical conversion of CO_2 to useful chemicals: current status, remaining challenges, and future opportunities. *Curr. Opin. Chem. Eng.* **2**, 191–199 (2013).
2. Wakerley, D. et al. Bio-inspired hydrophobicity promotes CO_2 reduction on a Cu surface. *Nat. Mater.* **18**, 1222–1227 (2019).
3. Wang, H. et al. Synergistic enhancement of electrocatalytic CO_2 reduction to C_2 oxygenates at nitrogen-doped nanodiamonds/Cu interface. *Nat. Nanotechnol.* **15**, 131–137 (2020).
4. Phillips, K. R., Katayama, Y., Hwang, J. & Shao-Horn, Y. Sulfide-derived copper for electrochemical conversion of CO_2 to formic acid. *J. Phys. Chem. Lett.* **9**, 4407–4412 (2018).
5. Ren, R. et al. Molecular electrocatalysts can mediate fast, selective CO_2 reduction in a flow cell. *Science* **365**, 367–369 (2019).
6. Wu, Y., Jiang, Z., Lu, X., Liang, Y. & Wang, H. Domino electroreduction of CO_2 to methanol on a molecular catalyst. *Nature* **575**, 639–642 (2019).
7. Xia, C. et al. Continuous production of pure liquid fuel solutions via electrocatalytic CO_2 reduction using solid-electrolyte devices. *Nat. Energy* **4**, 776–785 (2019).
8. Lum, Y. & Ager, J. W. Evidence for product-specific active sites on oxide-derived Cu catalysts for electrochemical CO_2 reduction. *Nat. Catal.* **2**, 86–93 (2019).
9. Dinh, C.-T. et al. CO_2 electroreduction to ethylene via hydroxide-mediated copper catalysis at an abrupt interface. *Science* **360**, 783–787 (2018).
10. Li, F. et al. Molecular tuning of CO_2-to-ethylene conversion. *Nature* **577**, 509–513 (2019).
11. Gregorio, G. L. D. et al. Facet-dependent selectivity of Cu catalysts in electrochemical CO_2 reduction at commercially viable current densities. *ACS Catal.* **10**, 4854–4862 (2020).
12. Wang, X. et al. Efficient electrically powered CO_2-to-ethanol via suppression of deoxygenation. *Nat. Energy* **5**, 478–486 (2020).
13. Stephens, I. E. L. et al. 2022 roadmap on low temperature electrochemical CO_2 reduction. *J. Phys. Energy* **4**, 042003 (2022).
14. Sisler, J. et al. Ethylene electrosynthesis: a comparative techno-economic analysis of alkaline vs membrane electrode assembly *vs* CO_2–CO–C_2H_4 tandems. *ACS Energy Lett.* **6**, 997–1002 (2021).
15. Alerte, T. et al. Downstream of the CO_2 electrolyzer: assessing the energy intensity of product separation. *ACS Energy Lett.* **6**, 4405–4412 (2021).
16. Verma, S. et al. Insights into the low overpotential electroreduction of CO_2 to CO on a supported gold catalyst in an alkaline flow electrolyzer. *ACS Energy Lett.* **3**, 193–198 (2018).
17. Dinh, C.-T., de Arquer, F. P. G., Sinton, D. & Sargent, E. H. High rate, selective, and stable electroreduction of CO_2 to CO in basic and neutral media. *ACS Energy Lett.* **3**, 2835–2840 (2018).
18. Yan, Z., Hitt, J. L., Zeng, Z., Hickner, M. A. & Mallouk, T. E. Improving the efficiency of CO_2 electrolysis by using a bipolar membrane with a weak-acid cation exchange layer. *Nat. Chem.* **13**, 33–40 (2021).
19. Ooka, H., Figueiredo, M. C. & Koper, T. M. Competition between hydrogen evolution and carbon dioxide reduction on copper electrodes in mildly acidic media. *J. Am. Chem. Soc.* **33**, 9307–9313 (2017).
20. Wu, Y. et al. Electrochemical CO_2 reduction using gas diffusion electrode loading Ni-doped covalent triazine frameworks in acidic electrolytes. *Electrochem.* **88**, 359–364 (2020).
21. Bondue, C. J., Graf, M., Goyal, A. M. & Koper, T. M. Suppression of hydrogen evolution in acidic electrolytes by electrochemical CO_2 reduction. *J. Am. Chem. Soc.* **143**, 279–285 (2021).
22. Huang, J. E. et al. CO_2 electrolysis to multicarbon products in strong acid. *Science* **372**, 1074–1078 (2021).
23. Monteiro, M. C. O., Philips, M. F., Schouten, K. J. P. & Koper, T. M. Efficiency and selectivity of CO_2 reduction to CO on gold gas diffusion electrodes in acidic media. *Nat. Commun.* **12**, 4943 (2021).
24. Yang, K. et al. Cation-driven increases of CO_2 utilization in a bipolar membrane electrode assembly for CO_2 electrolysis. *ACS Energy Lett.* **6**, 4291–4298 (2021).
25. Gu, J. et al. Modulating electric field distribution by alkali cations for CO_2 electroreduction in strongly acidic medium. *Nat. Catal.* **5**, 268–276 (2022).
26. Xie, Y. et al. High carbon utilization in CO_2 reduction to multi-carbon products in acidic media. *Nat. Catal.* **5**, 564–570 (2022).
27. Verma, S., Lu, S. & Kenis, P. J. A. Co-electrolysis of CO_2 and glycerol as a pathway to carbon chemicals with improved technoeconomics due to low electricity consumption. *Nat. Energy* **4**, 466–474 (2019).
28. Li, T., Cao, Y., He, J. & Berlinguette, C. P. Electrolytic CO_2 reduction in tandem with oxidative organic chemistry. *ACS Cent. Sci.* **3**, 778–783 (2017).
29. Na, J. et al. General technoeconomic analysis for electrochemical coproduction coupling carbon dioxide reduction with organic oxidation. *Nat. Commun.* **10**, 5193 (2019).
30. Yadegari, H. et al. Glycerol oxidation pairs with carbon monoxide reduction for low-voltage generation of C_2 and C_3 product streams. *ACS Energy Lett.* **6**, 3538–3544 (2021).
31. Vehrenberg, J., Baessler, J., Decker, A., Keller, R. & Wessling, M. Paired electrochemical synthesis of formate via oxidation of glycerol and reduction of CO_2 in a flow cell reactor. *Electrochem. Commun.* **151**, 107497 (2023).
32. Monteiro, M. C. O. et al. Absence of CO_2 electroreduction on copper, gold and silver electrodes without metal cations in solution. *Nat. Catal.* **4**, 654–662 (2021).

33. Arceo, E., Marsden, P., Bergman, R. G. & Ellman, J. A. An efficient didehydroxylation method for the biomass-derived polyols glycerol and erythritol. Mechanistic studies of a formic acid-mediated deoxygenation. *Chem. Commun*. 3357–3359 (2009).
34. Sun, D., Yamada, Y., Sato, S. & Ueba, W. Glycerol as a potential renewable raw material for acrylic acid production. *Green Chem.* **19**, 3186–32213 (2017).
35. Jiang, Z. et al. Molecular catalyst with near 100% selectivity for CO_2 reduction in acidic electrolytes. *Adv. Energy Mater.* **13**, 2203603 (2023).

Acknowledgements

This work was supported by the Natural Sciences and Engineering Research Council (NSERC) of Canada and the Ontario Research Fund – Research Excellence programme. D.S. acknowledges the NSERC E. W. R. Steacie Memorial Fellowship. The authors thank R. Wolowiec and D. Kopilovic for their kind technical assistance. Electron microscopy characterization was performed at the Open Centre for the Characterization of Advanced Materials (OCCAM) in University of Toronto.

Author contributions

E.H.S. supervised the project. X.W. conceived the idea and designed the experiments. P.L. prepared the samples and carried out the electrochemical experiments. J.T. and J.Y.H. contributed to the SEM and TEM characterization. X.W., C.P.O., K.X. and J.W. did the analysis of energy consumption. A.S.R. carried out XPS measurements. X.W. and Y.L. performed XRD measurements. X.W., P.L. and E.H.S. co-wrote the manuscript. R.K.M., A.O. and D.S. assisted with the discussions. All authors discussed the results and assisted during manuscript preparation.

Competing interests

The authors declare no competing interests.

Additional information

Supplementary information The online version contains supplementary material available at https://doi.org/10.1038/s41893-024-01363-1.

Correspondence and requests for materials should be addressed to Edward H. Sargent.

Peer review information *Nature Sustainability* thanks Ki Tae Nam and the other, anonymous, reviewer(s) for their contribution to the peer review of this work.

nature portfolio

Corresponding author(s): Edward H. Sargent

Last updated by author(s): April 21, 2024

Reporting Summary

Nature Portfolio wishes to improve the reproducibility of the work that we publish. This form provides structure for consistency and transparency in reporting. For further information on Nature Portfolio policies, see our Editorial Policies and the Editorial Policy Checklist.

Statistics

For all statistical analyses, confirm that the following items are present in the figure legend, table legend, main text, or Methods section.

n/a	Confirmed	
☐	☒	The exact sample size (*n*) for each experimental group/condition, given as a discrete number and unit of measurement
☐	☒	A statement on whether measurements were taken from distinct samples or whether the same sample was measured repeatedly
☒	☐	The statistical test(s) used AND whether they are one- or two-sided *Only common tests should be described solely by name; describe more complex techniques in the Methods section.*
☒	☐	A description of all covariates tested
☒	☐	A description of any assumptions or corrections, such as tests of normality and adjustment for multiple comparisons
☐	☒	A full description of the statistical parameters including central tendency (e.g. means) or other basic estimates (e.g. regression coefficient) AND variation (e.g. standard deviation) or associated estimates of uncertainty (e.g. confidence intervals)
☒	☐	For null hypothesis testing, the test statistic (e.g. *F*, *t*, *r*) with confidence intervals, effect sizes, degrees of freedom and *P* value noted *Give P values as exact values whenever suitable.*
☒	☐	For Bayesian analysis, information on the choice of priors and Markov chain Monte Carlo settings
☒	☐	For hierarchical and complex designs, identification of the appropriate level for tests and full reporting of outcomes
☒	☐	Estimates of effect sizes (e.g. Cohen's *d*, Pearson's *r*), indicating how they were calculated

Our web collection on statistics for biologists contains articles on many of the points above.

Software and code

Policy information about availability of computer code

Data collection	No commercial, open source and custom code is used to collect the data in this study.
Data analysis	No commercial, open source and custom code is used to analyse the data in this study.

For manuscripts utilizing custom algorithms or software that are central to the research but not yet described in published literature, software must be made available to editors and reviewers. We strongly encourage code deposition in a community repository (e.g. GitHub). See the Nature Portfolio guidelines for submitting code & software for further information.

Data

Policy information about availability of data

All manuscripts must include a data availability statement. This statement should provide the following information, where applicable:

- Accession codes, unique identifiers, or web links for publicly available datasets
- A description of any restrictions on data availability
- For clinical datasets or third party data, please ensure that the statement adheres to our policy

All data are available within the paper, Supplementary Information, and Source Data file.

Human research participants

Policy information about studies involving human research participants and Sex and Gender in Research.

Reporting on sex and gender	Reporting on sex and gender was not relevant to the study.
Population characteristics	Population characteristic was not relevant to the study.
Recruitment	Recruitment was not relevant to the study.
Ethics oversight	Ethics oversight was not relevant to the study.

Note that full information on the approval of the study protocol must also be provided in the manuscript.

Field-specific reporting

Please select the one below that is the best fit for your research. If you are not sure, read the appropriate sections before making your selection.

☐ Life sciences ☐ Behavioural & social sciences ☒ Ecological, evolutionary & environmental sciences

For a reference copy of the document with all sections, see nature.com/documents/nr-reporting-summary-flat.pdf

Ecological, evolutionary & environmental sciences study design

All studies must disclose on these points even when the disclosure is negative.

Study description	CO and acrolein coproduction via paired electrolysis
Research sample	Electrode sources: gas diffusion electrode (Sigracet 39 BB, Fuel Cell Store); Ag catalysts (99.99 % Ag target, sputtering rate about 1 Å s-1); Ti fibre felts (Fuel Cell Store); commercial carbon-supported metal nanoparticles (60 wt.% Pt on vulcan XC-72R, Fuel Cell Store, 4-5 nm; 60 wt.% Pd on Vulcan XC-72R, Fuel Cell Store, 6-8 nm; 40 wt.% Ru on vulcan XC-72R, Fuel Cell Store, 4-6 nm; or 40 wt.% Au on Ketjenblack, Fuel Cell Store, 3-6 nm); Nafion perfluorinated resin solution (5 wt.%, Sigma-Aldrich)
Sampling strategy	Electrode preparation: The cathode electrode was prepared by sputtering Ag with different thickness onto a piece of carbon paper gas diffusion electrode (GDE) (Sigracet 39 BB, Fuel Cell Store) at a rate of 1 Å s-1 by using a pure Ag target (99.99 %). To fabricate the anode electrode, we first etched the Ti fibre felts (Fuel Cell Store) in a 10 wt.% oxalic acid aqueous solution at 98°C for 40 min. The etched Ti fibre felts were washed by deionized (DI) water and then dried at room temperature. Commercial carbon-supported metal nanoparticles (60 wt.% Pt on vulcan XC-72R, Fuel Cell Store, 4-5 nm; 60 wt.% Pd on Vulcan XC-72R, Fuel Cell Store, 6-8 nm; 40 wt.% Ru on vulcan XC-72R, Fuel Cell Store, 4-6 nm; or 40 wt.% Au on Ketjenblack, Fuel Cell Store, 3-6 nm) were dispersed in the mixture of DI water, isopropanol, and Nafion perfluorinated resin solution (5 wt.%, Sigma-Aldrich) and ultrasonicated for 90 minutes. The well-dispersed suspension was then spray coated on Ti fibre felts to prepare anode electrodes with different metal loadings. Electrochemical measurements: The electrochemical measurements were conducted using an electrochemical station (AUT5113) with a two-electrode system in a flow cell. Cathode electrodes, cation exchange membrane (Nafion 117, Fuel Cell Store), and anode electrodes were positioned and clamped together via polytetrafluoroethylene gaskets. The geometric area of the cathode electrode in the flow cell is 0.5 cm2. In the CO2RR-OER system, 3 M KCl aqueous solution with different pHs adjusted by H2SO4 and 0.05 M KOH aqueous solution were introduced into the cathode chamber and anode chamber, respectively. In the CO2RR-AOR system, 3 M KCl aqueous solution adjusted by H2SO4 to pH 1 as catholyte and different concentrations of allyl alcohol in KOH aqueous solution/ different concentrations of H2SO4/K2SO4 as anolyte were introduced into the cathode chamber and anode chamber, respectively. The electrolytes were circulated using peristaltic pumps at the rate of 5 mL min-1. CO2 gas (Linde, 99.99%) was continually supplied to the gas chamber of the flow cell during CO2RR (without specification, the CO2 feed rate is 20 mL min-1). A gas chromatograph (Shimadzu GC-2014ATF) equipped with thermal conductivity and flame ionization detectors was used to examine the CO2RR gas products. NMR spectrometer (Agilent DD2 600 MHz) was used to analyze the liquid products generated in cathodic CO2RR and anodic allyl alcohol oxidation with dimethylsulfoxide as an internal standard. Combined with NMR results, GC-MS (Thermo ISQ7000) was further used to analyze all the liquid products generated in anodic allyl alcohol oxidation. The acrolein and acrylic acid/acrylate produced in anodic AOR were quantified using a HPLC (Thermo Scientific DIONEX UltiMate 3000; Aminex HPX-87H 300 × 7.8 mm column) with an aqueous solution of 0.005 M H2SO4 as eluate.
Data collection	All data were collected from related instruments by authors.
Timing and spatial scale	Start date: Oct. 25, 2021; End date: Feb. 15, 2024
Data exclusions	No data were excluded from the analysis.
Reproducibility	The repeated experiments were performed to confirm the reproducibility of experimental findings, and all attempts to repeat the experiment were successful.
Randomization	All samples were allocated into groups to the design of related experiments.

Blinding | Blinding was not relevant to the study.

Did the study involve field work? ☐ Yes ☒ No

Reporting for specific materials, systems and methods

We require information from authors about some types of materials, experimental systems and methods used in many studies. Here, indicate whether each material, system or method listed is relevant to your study. If you are not sure if a list item applies to your research, read the appropriate section before selecting a response.

Materials & experimental systems

n/a	Involved in the study
☒	☐ Antibodies
☒	☐ Eukaryotic cell lines
☒	☐ Palaeontology and archaeology
☒	☐ Animals and other organisms
☒	☐ Clinical data
☒	☐ Dual use research of concern

Methods

n/a	Involved in the study
☒	☐ ChIP-seq
☒	☐ Flow cytometry
☒	☐ MRI-based neuroimaging